Modeling of the optical piston: Density-wave shape and resonance-fluorescence effects

J. M. Calo,* N. M. Lawandy, D. Frezzo, and M. T. Perkins
Division of Engineering, Brown University, Providence, Rhode Island 02912
(Received 8 February 1988; revised manuscript received 11 April 1988)

We present results of a numerical model of the optical piston driven by laser-induced drift (LID). The model is based on a drift-velocity formulation of Lawandy, derived from an asymmetric-random-walk argument, and includes resonance-fluorescence effects. The model is applied primarily to the experimental conditions of H. G. C. Werij and co-workers [Phys. Rev. A **33**, 3270 (1986)]. It is shown that both the velocity and the shape of the propagating density wave change continuously throughout the traverse of a (finite) diffusion tube under these conditions. In addition, we have numerically verified the contention of G. Nienhuis [Phys. Rev. A **31**, 1636 (1985)] that a "self-preserving" form of the density wave is indeed possible for the case of a "finite number of absorbers in an infinite medium," both with and without saturation. Finally, we show that resonance fluorescence slows the piston velocity, broadens the density distribution, and decreases its peak height. It is concluded that resonance fluorescence can play a significant role in determining the time evolution and detailed shape of the optical-piston density distribution in sodium.

I. INTRODUCTION

Recently, there has been significant interest in the experimental and analytical investigation of the phenomenon of light-induced drift (LID). In the work of Werij *et al.*,[1,3] Na in its $3S$ ground state in an argon buffer gas was excited near the Na D_2 resonance to its $3P$ level. Off-line-center excitation results in the production of counter-diffusion fluxes of excited- and ground-state Na. Since the diffusion cross section of the excited-state species is generally larger than that of its ground-state counterpart, these fluxes will not be equal. Thus, an initial δ-function packet of Na, excited in this manner, will exhibit asymmetric diffusion in the direction away from that of the velocity group selected. Therefore, for axial excitation in a cylindrical tube, a net Na flux will occur away from the laser source when the latter is tuned to the red Doppler wing, and vice versa. The asymmetry of the diffusion process gives rise to a time-dependent expectation value of the first moment of the density distribution, which is manifested as a drift velocity v_d; hence the name light-induced drift. In an optically thick system, this behavior results in the formation and propagation of a density wave that literally sweeps the gas mixture of the absorbing species. It is this latter phenomenon that has been given the name of the *optical piston* by Werij *et al.*[1-3]

The prediction of this phenomenon seems to have originated with the work of Gel'mukhanov and Shalagin.[4,5] More recent interest has been provided by the elegant experimental work of Werij and co-workers[1-3] involving the Na optical piston in a gehlinite glass tube. In this latter work, it was also hypothesized that the piston velocity is a strong function of Na adsorption on the tube walls. This was subsequently verified by experimental results which demonstrate that the piston velocity can be substantially increased by coating the tube walls to minimize Na adsorption (Werij *et al.*[6] and Xu *et al.*[7]). A rubidium optical piston (i.e., Rb in argon) has also been demonstrated (Hamel *et al.*[8]).

Due to the nature of LID, it has obvious potential applications as a separation technique for removing low levels of impurities, and for isotope separation. The direct effect of wall interaction on the velocity of the optical piston has also been suggested as a surface diagnostic technique. In addition, of course, LID phenomena provide very useful information on intermolecular potentials and gas kinetic theory in a conveniently observable macroscopic form.

In the current paper we present a numerical model of the optical piston and report on results obtained for conditions similar to that employed in the experimental work of Werij *et al.*,[2] hereafter known as WHW. In particular, we examine the effects of resonance fluorescence on the shape and behavior of the optical piston.

II. MODEL DEVELOPMENT

A. Drift velocity

An expression for the drift velocity v_d, based on a random walk argument, has been derived by Lawandy.[9] The result of this derivation for a two-level absorber in a one-dimensional system is

$$v_d=(\lambda_g/\tau_c)[\alpha\beta/(\alpha+\beta)]\ln(\alpha/\beta)\ , \tag{1}$$

where α and β are ratios of the effective mean free paths of the absorber in the ($\pm$) directions to the mean free path of a ground-state species λ_g, and τ_c is the mean collision time. α and β are further given by

$$\alpha=1-P_e^{+}(1-\lambda_e/\lambda_g)\ , \tag{2a}$$

$$\beta=1-P_e^{-}(1-\lambda_e/\lambda_g)=1-\delta\ , \tag{2b}$$

where $P_e^{\pm}$ are the probabilities for an excited species to be moving in the ($\pm$) directions, and λ_e is the mean free path

of an absorber in the excited state.

Neglecting the effects of fluorescence, for the time being, and for excitation of the red wing from the (−) direction, $P_e^+=0$ and $\alpha=1$, whereupon v_d becomes

$$v_d=(\lambda_g/\tau_c)[\beta/(1+\beta)]\ln(1/\beta)\ . \tag{3}$$

β is given by Eq. (2b), from which $\delta=P_e^-(1-\lambda_e/\lambda_g)$, and

$$P_e^-=(\tfrac{1}{2})(\ln 2/\pi)^{1/2}(\Delta\nu_h/\Delta\nu_D)(I/I_s)/(1+I/I_s)^{1/2}\ , \tag{4}$$

where $\Delta\nu_h$ and $\Delta\nu_D$ are the homogeneous and Doppler linewidths, respectively, and I and I_s are the local laser and saturation intensities, respectively. Since for typical operating values of the parameters $\delta\ll 1$, Eq. (3) becomes

$$v_d=(\lambda_g/\tau_c)[(1-\delta)/(2-\delta)]\delta\approx(\tfrac{1}{2})(\lambda_g/\tau_c)\delta\ . \tag{5}$$

It is noted that this expression is of the exact same form, with respect to the laser intensity I as given by WHW Eq. (9). In fact, even the predicted values are quite similar; e.g., for the experimental conditions of WHW presented in Table I(a), WHW Eq. (15) yields $v_d(0)=320$ cm/s for the drift velocity at the incident laser power, $I_0=1.6$ W/cm^2, whereas Eq. (5) yields 318 cm/s. Thus, the two expressions appear to be equivalent. Equation (5), however, allows for the facile inclusion of resonance fluorescence effects, as demonstrated below.

If it is assumed that the resonance-fluorescence intensity $I_f(z)$ interacts with the entire absorber velocity distribution, then for red wing excitation originating at $z=0$, $P_e^{\pm}$ can be approximated as

$$P_e^+=(\tfrac{1}{4})[(I_f/I_s)/(1+I_f/I_s)]\ , \tag{6a}$$

$$P_e^-=P_e^+ +[(\tfrac{1}{2})-2P_e^+](\ln 2/\pi)^{1/2}(\Delta\nu_h/\Delta\nu_D)(I/I_s)/(1+I/I_s)^{1/2}\ . \tag{6b}$$

An examination of Eqs. (6a) and (6b) reveals that $P_e^->P_e^+$, or $\alpha>\beta$, or from Eq. (1), $v_d>0$, i.e., drift in the positive z direction for red wing excitation from a source located at $z=0$. It is also noted that these expressions observe the correct expected limits; i.e., P_e^- reduces to Eq. (4) for $I_f=0$ (i.e., $P_e^+=0$), and $P_e^-\to P_e^+$ (i.e., $\beta\to\alpha$), or $v_d\to 0$ as I_f becomes large. From the latter, it is evident that the primary qualitative effect of increasing fluorescence intensity is to reduce the effective local drift velocity by decreasing the population of the selected velocity group. It will be shown below that, in general, the effects of resonance fluorescence are to broaden and slow the density wave in the case of the optical piston.

B. Macroscopic continuity expressions

The one-dimensional continuity expression for the absorber species in a buffer gas for LID, as given by WHW, is

$$\partial n/\partial t=D_g\partial^2 n/\partial z^2-\partial(nv_d)/\partial z\ , \tag{7}$$

where $n(z,t)=n_g(z,t)+n_e(z,t)$ is the local absorber number density (the subscripts g and e designate ground- and excited-state species, respectively, for the two-level system), and D_g is the effective diffusivity of the ground state. In dimensionless form, Eq. (7) becomes

$$\partial\rho/\partial\theta=\partial^2\rho/\partial\zeta^2-\gamma\partial[\rho v]/\partial\zeta\ , \tag{8}$$

where $\theta=tD_g/L^2$, $\rho=n/n_0$, $\zeta=z/L$, $\gamma=v_d(0)L/D_g$ (the characteristic Péclet number for the system), n_0 is the initial mean density in the diffusion cell, L is the tube length, $v_d(0)$ is the drift velocity at $z=0$, and $v=v_d/v_d(0)$.

The laser intensity is coupled to Eq. (8) via the saturated form of the Beer-Lambert law:

$$\partial I/\partial z=-\sigma_a n(z)I(z)/(1+I/I_s)^{1/2}\ , \tag{9}$$

which in dimensionless form becomes

$$\partial(I/I_s)/\partial\zeta=-\alpha\rho(\zeta)(I/I_s)/(1+I/I_s)^{1/2}\ , \tag{10}$$

where $\alpha=\sigma_a n_0 L$. Equation (10) can be integrated directly to yield

$$2(y-y_0)+\ln\{[(y-1)(y_0+1)]/[(y_0-1)(y+1)]\}=-\alpha\xi\ , \tag{11}$$

where $y=(1+I/I_s)^{1/2}$ and $y_0=(1+I_0/I_s)^{1/2}$, and

$$\xi=\int_0^{\zeta}\rho\,d\zeta' \tag{12}$$

is the axial column density. The transcendental equation (11) can be solved for y (i.e., I) using standard numerical root-finding techniques.

The axial column density [Eq. (12)] provides a useful transformation for the mass continuity expression, Eq. (8), which simplifies the numerical solution scheme and the boundary conditions. Integrating Eq. (8) with respect to ζ, and noting that $\rho=d\xi/d\zeta$, transforms it to

$$\partial\xi/\partial\theta=\partial^2\xi/\partial\zeta^2-\gamma v\partial\rho/\partial\zeta\ , \tag{13}$$

which is the actual expression that was solved numerically, rather than the density expression directly.

C. Boundary conditions

For the geometry employed in the experiments of WHW, the laser radiation was introduced axially at the end of the diffusion cell away from the Na reservoir appendage [i.e., at z (or ζ)$=0$], at which it is obvious that $\xi=0$.

The other end of the cell is more interesting. At first it may appear that the diffusion cell is a closed system, and that the appropriate condition would be $\xi=1$. However, the Na reservoir in the appendage acts as a source-sink for Na, and thus the cell is actually open at this end with respect to Na (but obviously closed with respect to the buffer gas Ar). Due to the relatively low value of the piston velocity in the work of WHW, it may be safely assumed that the Na vapor and liquid are in equilibrium immediately above the surface of the molten Na source. It is noted that the Na reservoir was located at some distance from the end of the diffusion cell. Therefore, for calculation purposes here, the cell length was taken as 15 cm (as given by WHW), with an additional estimated length of 5 cm to account for the separation of the Na reservoir from the actual end of the diffusion cell. (In any case, the results of the simulations are relatively insensitive to this latter value.) Thus, the entire cell length is taken as $L=20$ cm, divided into two regions: a 15-cm-long diffusion cell in which diffusion and drift operate simultaneously in accordance with Eq. (8), and a 5-cm-long region between the end of the diffusion cell and the Na reservoir, in which only ordinary diffusion operates.

In summary then, the most appropriate boundary conditions for the experimental conditions of WHW are

$$\xi=0 \quad \text{at } \zeta=0 \text{ (laser entrance)} , \tag{14a}$$

$$\partial\xi/\partial\zeta=\rho=\epsilon \quad \text{at } \zeta=1 \text{ (Na reservoir)} , \tag{14b}$$

where $\epsilon=n_{\text{res}}/n_0=1$ if the vapor pressure above the liquid Na is maintained at n_0, or some other appropriate value if it is not.

D. Fluorescence

The effect of fluorescence on the drift velocity can be determined using the formulation of Eq. (3). In order to apply this expression, however, an estimate of the local fluorescence intensity must be made. Obtaining an exact solution to this problem is difficult due to complications caused by radiation imprisonment or trapping, which is likely to occur at the high densities and energy fluences that have been used to demonstrate the optical piston. For example, the absorption cross section for fluorescence over the entire line is given by WHW as

$$\sigma=h\omega/4\pi I_s\tau , \tag{15}$$

where $\tau=16$ ns is the spontaneous lifetime of the Na D_2 line, $h\omega/2\pi=3.37\times10^{-19}$ J, and $I_s=0.27$ W/cm^2. This expression yields $\sigma=3.9\times10^{-11}$ cm^2. For a peak absorber density of 7×10^{12} cm^{-3}, the absorption length is $1/\sigma n=3.7\times10^{-3}$ cm, which is much smaller than the radius of the 1-mm capillary used by WHW. Obviously, radiation trapping is a certainty under these conditions.

An estimate of the local fluorescence intensity was obtained as follows. Due to the high quantum efficiency of the Na D_2 line, practically all the absorbed radiation must be re-emitted as fluorescence. Also, due to the rapid time scale of photon transport in comparison to that of the piston, it is reasonable to assume steady state locally with respect to the fluorescence intensity. With these assumptions in mind, and neglecting axial radiative losses in comparison to those in the radial direction (due to the generally low probability of leakage from the tube in the axial direction), a simple energy balance over a differential volume element yields

$$I_f/I_s=-(d/4T)d(I/I_s)/dz , \tag{16}$$

where d is the tube diameter and T its transmissivity to fluorescence radiation. The actual transmissivity of the tube used in the experiments of WHW is not known, and by its inclusion in Eq. (16) we do not intend to imply that it was anything other than unity. However, T serves as a convenient control parameter with which to vary the fluorescence intensity in order to examine its effect on the drift velocity (see Sec. III below). In dimensionless form, Eq. (16) becomes

$$I_f/I_s=(d/4LT)\alpha\rho(\xi)(I/I_s)/(1+I/I_s)^{1/2} . \tag{17}$$

This is the expression that is used in the current model to estimate the fluorescence intensity for inclusion in Eq. (1) for the drift velocity.

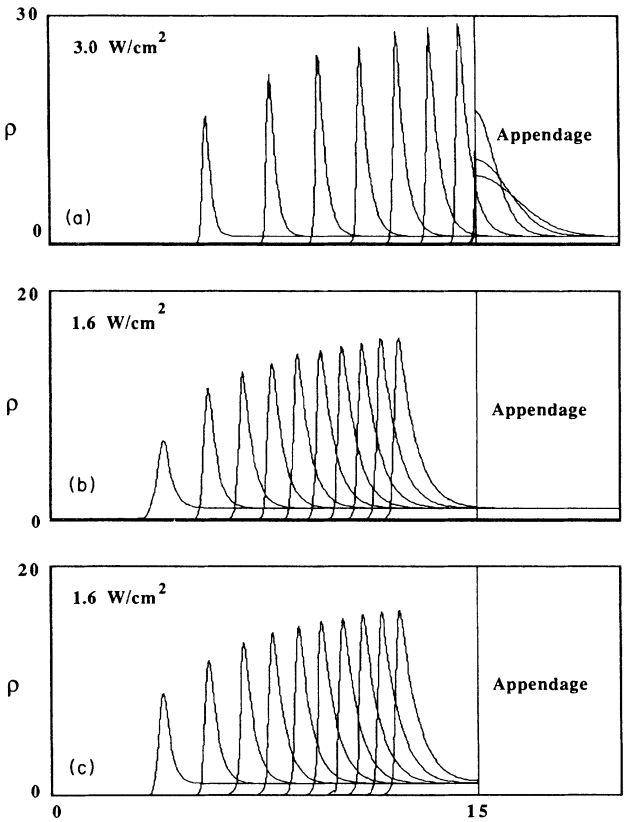

FIG. 1. Number density distributions for optical-piston propagation calculated using the model proposed by WHW (Ref. 2) *without* resonance-fluorescence effects for equal time intervals of $\theta=10^{-2}$. (a) $I_0=3.0$ W/cm^2 with boundary conditions (14a) and (14b); $\alpha=40,\gamma=454$; (b) $I_0=1.6$ W/cm^2 with boundary conditions (14a) and (14b); $\alpha=40,\gamma=320$; (c) $I_0=1.6$ W/cm^2 with an impenetrable boundary at $\zeta=1;\alpha=30,\gamma=320$. (Note that the equivalent time step for the latter calculation is $\theta=1.78\times10^{-2}$.)

TABLE I. Experimental values and dimensionless model parameters for the experiments of WHW (Ref. 2).

	(a)	(b)
I_0, incident laser intensity (W/cm^2)	1.6	3.0
$v_d(0)$ (cm/s) [WHW Eq. (15)]	320	454
α (20-cm cell length) $(=\sigma_a n_0 L)$	40	40
α (15-cm cell length)	30	30
γ (20-cm cell length) $[=v_d(0)L/D_g]$	320	454
γ (15-cm cell length)	240	340.5
Characteristic time (s) $(=L^2/D_g)$; $L=20$ cm	20	20
WHW (Ref. 2) experimental and estimated parameter values		
I_s, Na D_2 line saturation intensity (W/cm^2)	0.27	
D_g (cm^2/s)	20	
σ_a (cm^2)	2×10^{-12}	
n_0 (cm^{-3})	1×10^{12}	
T_{cap} (K)	520	

III. RESULTS AND DISCUSSION

All the numerical results in this section were obtained by integration of the corresponding model using the package PDECOL (Madsen and Sincovec[10]) which is a general code for the solution of systems of coupled partial differential equations in one time and one space dimension. The principal technique is finite element collocation over piecewise polynomials expressed in terms of B-spline basis functions for spatial discretization. As applied in the current work, the code was used to solve a system of only one PDE, the integrated form of the macroscopic continuity equation (13). However, it was also necessary to simultaneously solve the nonlinear algebraic expressions for the laser intensity [Eq. (11)] and the fluorescence intensity [Eq. (17)] in order to obtain the local value of the drift velocity [Eq. (1)].

A. Model results without fluorescence

Numerical solutions were first obtained for the model as presented by WHW [i.e., WHW Eq. (8)] with no resonance fluorescence effects. The results of these calculations are presented in Figs. 1(a) and 1(b) for the experimental conditions of WHW listed in Table I(a) and I(b), respectively. For these calculations, the drift velocity $v_d(z)$ was determined from WHW Eq. (9). The boundary conditions used in these calculations were (14a) and (14b) with $\epsilon=1$. As long as the density wave does not interact strongly with the end of the cell at $z=15$ cm, the numerical results are relatively insensitive to the end boundary condition (14b). In order to demonstrate this, results for the exact same conditions as given in Fig. 1(b) are presented in Fig. 1(c) for a closed cell with $\xi=1$ at $\zeta=1$ (i.e., at $z=15$ cm) in lieu of condition (14b). As shown, the results are quite similar.

Due to the similarity of the limiting form of Eq. (1) for the experimental conditions of WHW [i.e., Eq. (5)] to WHW Eq. (9), as discussed in Sec. II A above, it is to be expected that numerical results would also be comparable. Indeed, results from calculations using our current formulation for the drift velocity were virtually indistinguishable from those presented in Fig. 1.

Some interesting observations can be derived from the numerical results presented in Fig. 1. In Fig. 2 are plotted the first three moments of the Na density wave for the WHW model results of Fig. 1(b). As is evident, the first moment increases in a monotonic, nonlinear fashion indicative of continuous deceleration of the density wave as it progresses through the capillary. This behavior is not consistent with the assumption of the piston attaining a constant velocity v_p as applied by WHW in their analysis. It is also inconsistent with some of the data (e.g., WHW Fig. 5a) which clearly show that after a brief initial period of relatively constant velocity, the piston de-

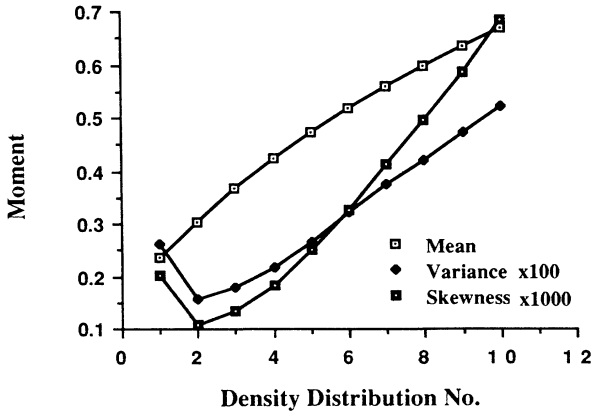

FIG. 2. First (noncentral), and second and third central moments of the ten-number density distributions presented in Fig. 1(b).

celerates for a time, and then actually accelerates smoothly to the end of the cell.

The second and third moment results presented in Fig. 2 also show that after an initial sharpening associated with the formation of the density wave, the variance and skewness of the optical piston both increase monotonically throughout its traverse of the capillary. This behavior is not consistent with the piston attaining a self-preserving form. In addition, as is evident from Fig. 1, the peak amplitude never attains a steady-state value, but rather progressively increases as the piston continuously accumulates additional Na.

The temporal development of the piston shape can be better appreciated by replotting the results of Fig. 1(b), as shown in Fig. 3(a). In this latter figure, the maxima of the ten density distributions of Fig. 1(b) have been normalized to unity and superimposed. As can be seen, the illuminated leading edge of the density distribution rapidly establishes a steady-state form, i.e., the shape of the leading edge does not change significantly after the second time step. The dark side of the distribution, however, continually broadens and increases in amplitude as the wave sweeps and accumulates sodium. Accumulation of sodium on the dark side of the distribution is also responsible for the slowing down of the density wave. WHW have shown experimentally that suddenly increasing the downstream density by heating the Na appendage causes the optical piston to stop and travel backwards. From these results, it is apparent that for the experimental conditions of WHW, where there is always sodium available to be swept in front of the density wave, the dark side of the density distribution will never assume a self-preserving form.

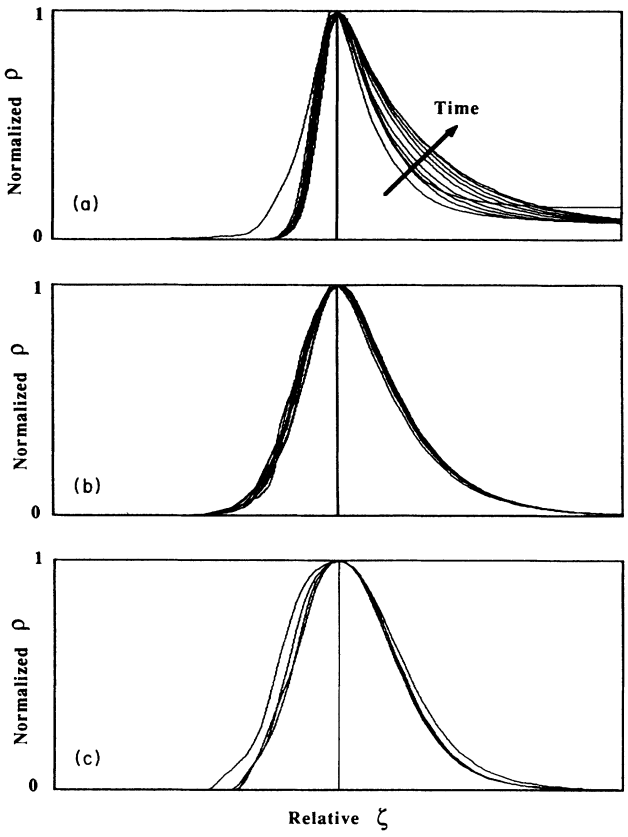

FIG. 3. Normalized and superimposed number density distributions for $\alpha=40, \gamma=320$ for equal time increments of $\theta=10^{-2}$. (a) Data of Fig. 1(b); (b) Eq. (18) model without saturation; (c) Eq. (13) model with saturation. (Note that due to the higher piston velocity observed in the latter case, only the first four density distributions are presented.)

The assumption of a self-preserving form for the Na optical piston derives from the analysis of Nienhuis.[11] However, Nienhuis's results were obtained for the specific case of a finite number of absorbers in an infinite medium. These conditions were not satisfied in the experiments of WHW.

In Fig. 3(b) it is shown numerically that a self-preserving form can indeed be attained under the conditions cited by Nienhuis. These results were obtained for the exact same parameters as in Fig. 3(a), using the unsaturated form of the Beer-Lambert law for the drift velocity, with the condition of a finite number of absorbers approximated by imposing an initial sodium distribution of density $\rho=1$ over only the first 10% of the diffusion tube, rather than along its entire length, as was done for the calculations presented in Fig. 1(b). As can be seen, the shape of the density wave is very nearly invariant over the entire piston evolution.

That similar behavior can be expected under saturated conditions is shown by the results presented in Fig. 3(c) which were obtained using the saturated form of the Beer-Lambert law [i.e., Eq. (10)] for the drift velocity. As in Fig. 3(b), it appears that after the first time increment, at which the distribution is slightly broader than the others, the form of the density wave remains relatively well preserved for the subsequent time increments shown. Only a total of four time increments, free of the effects of the far boundary, were recorded for the exact same time and parameter values as in Fig. 3(b) because one effect of saturation was to significantly increase the piston velocity such that subsequent density distributions were situated against the boundary of the cell at $\zeta=1$. A comparison of panels (b) and (c) indicates that saturation seems to slightly broaden the distributions near the peak, but reduces tailing somewhat on the dark side. These results graphically demonstrate that unsaturated conditions are not necessary in order for the density wave to assume a self-preserving form, as also implied by Nienhuis.[12]

B. Model results with fluorescence

In all our calculations using the model proposed by WHW (or other related models) to explain the propagation of the optical piston, we could not obtain density-wave shapes that were qualitatively very similar to the Na density profiles recorded by WHW. For example, the oscilloscope display obtained with a probe beam perpendicular to the diffusion tube, presented in WHW Fig. 4, shows a Na density profile that is significantly broader and of a lesser amplitude than those shown in Fig. 1. Therefore, it must be concluded that the model of WHW and the estimates obtained from the "self-preserving form" ideas of Nienhuis are, at best, only a first-order

representation of the actual behavior of the optical piston density wave. There must be other additional effects that cause the piston amplitude to dampen and its width to increase during its traverse of the diffusion cell. It is proposed here that at least one important effect that has not yet been explicitly considered is resonance fluorescence.

The effects of resonance fluorescence can be readily included in the numerical model via our formulation for the drift velocity [i.e., Eqs. (1), (3), and (6)], using Eq. (16) to estimate the fluorescence intensity, as discussed in Sec. II D above.

Results of calculations including resonance fluorescence for the two laser intensities used by WHW are presented in Figs. 4 and 5. The ten density distributions in each panel correspond to the exact same times in each case, i.e., each distribution occurs at increments of $\theta=10^{-3}$, for a total elapsed time of 10^{-2}. The results presented in panels 4(a) and 5(a) are reproductions of Figs. 1(a) and 1(b), respectively. The (b) panels in Figs. 4 and 5 were determined for a capillary wall transmissivity of unity, and the (c) panels represent the effects of increasing the resonance fluorescence by decreasing the transmissivity to one-half.

The effects of fluorescence are quite apparent. In both figures resonance fluorescence acts to significantly (1) slow the piston, (2) broaden each density distribution, and (3) decrease the peak intensities, in comparison to the nonfluorescence case presented in the corresponding panel (a). This is due, of course, to the effect discussed previously (i.e., in Sec. II A) that resonance fluorescence primarily serves to effectively depopulate the Doppler-selected velocity group, such that the laser radiation interacts with fewer absorbers. In a sense, this is similar to the role of wall adsorption, as discussed by Werij *et al.*,[1] WHW, Werij *et al.*,[6] and Xu *et al.*[7] In particular, in the work of WHW, it was concluded that approximately one hundred times as much Na was adsorbed on the walls of the gehlinite glass diffusion cell than was present in the buffer gas. Adopting a local equilibrium model with respect to wall adsorption, WHW concluded that the effective diffusivity, drift velocity, and actual piston velocity were given by

$$D_{g,\text{eff}}=D_g/(1+K)\ , \tag{18a}$$

$$v_{d,\text{eff}}=v_d/(1+K)\ , \tag{18b}$$

$$v_{p,\text{eff}}=v_p/(1+K)\ , \tag{18c}$$

where K is the equilibrium constant for wall adsorption.

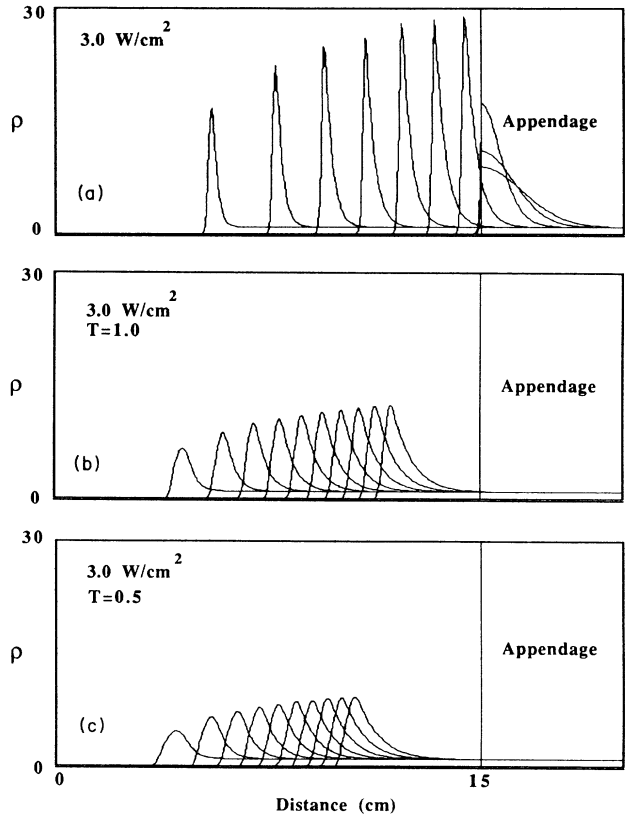

FIG. 4. Number density distributions for optical-piston propagation calculated using the current model [i.e., Eq. (3) for v_d, Eq. (13) with saturation, Eq. (16), and boundary conditions (14a) and (14b)] *with* resonance-fluorescence effects for $I_0=3.0$ W/cm^2; $\alpha=40,\gamma=454$; and equal time increments of $\theta=10^{-2}$. (a) Base case, Fig. 1(a); (b) $T=1.0$; (c) $T=0.5$.

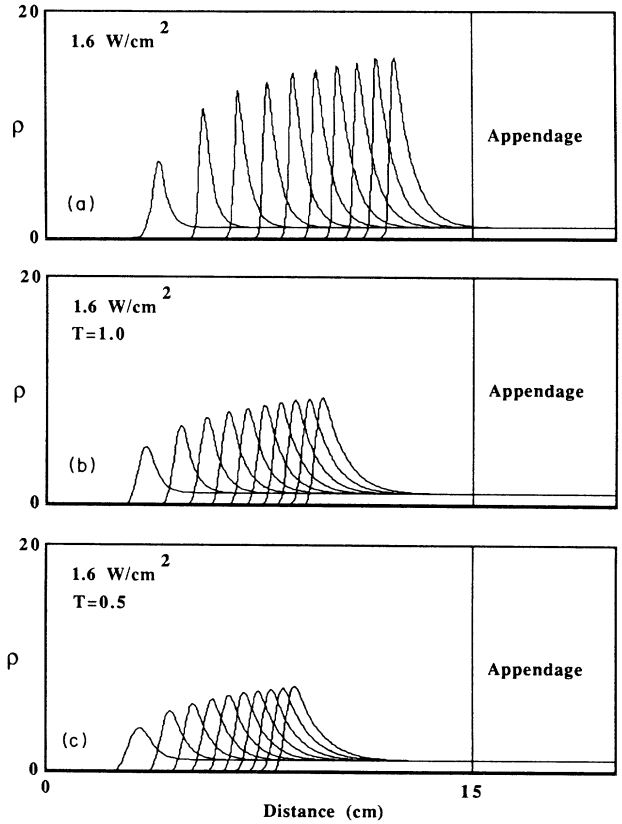

FIG. 5. Number density distributions for optical-piston propagation calculated using the current model [i.e., Eq. (3) for v_d, Eq. (13) with saturation, Eq. (16), and boundary conditions with (14a) and (14b)] *with* resonance-fluorescence effects for $I_0=1.6$ W/cm^2; $\alpha=40,\gamma=320$; and equal time increments of $\theta=10^{-2}$. (a) Base case, Fig. 1(b); (b) $T=1.0$; (c) $T=0.5$.

From the work of Werij *et al.*[6] and Xu *et al.*,[7] it is quite obvious that well adsorption plays a dominant role in controlling the magnitude of experimentally observed values of the piston velocity. Even so, however, there still remain significant discrepancies between predicted and measured piston velocities. For example, for the two cases presented in Table I (i.e., for $I_0=1.6$ and 3.0 W/cm^2), WHW Eq. (16) yields 28 and 53 cm/s, respectively, for v_p. WHW measured $D_{g,\text{eff}}=0.14$ cm^2/s. From Eq. (18a), for $D_g=20$ cm^2/s, $K\approx 142$. Employing expressions (18b) and (18c), this yields $v_{p,\text{eff}}\approx 0.2$ and 0.4 cm/s for the two respective cases. For $I_0=3$ W/cm^2, WHW report an experimental value of $v_{p,\text{eff}}\approx 0.1$ cm/s, i.e., a factor of 4 less than the value estimated from their analysis.

It is our thesis that resonance fluorescence can account for much of the difference between the actual and estimated values. For example, in Fig. 4 the difference between the apparent piston velocities towards the end of the diffusion cell for Figs. 4(a) and 4(b) is a factor of 2, i.e., 59 cm/s vs 30 cm/s, *without wall adsorption effects.* Assuming $K\approx 142$, according to WHW, the corresponding $v_{p,\text{eff}}$ are 0.4 cm/s and 0.2 cm/s. The latter value is obviously much closer to that observed experimentally.

The corresponding fluorescence distributions for Figs. 4(b) and 4(c) and 5(b) and 5(c) are presented in Figs. 6(a) and 6(b) and 7(a) and 7(b), respectively. As expected, the fluorescence distributions are much sharper than their corresponding density distributions for this optically thick system. The slowing-down behavior evident in Figs. 4 and 5 is also apparent, i.e., increasing fluorescence slows the piston. Also, the peak intensities of the fluorescence distributions increase with increasing fluorescence. It is interesting to note that although the peak fluorescence intensities fall just short of I_s in Fig. 7(a) (i.e., for $I_0=1.6$ W/cm^2), they significantly exceed I_s in Fig. 6(a) (i.e., for $I_0=3.0$ W/cm^2).

Of equal import to the apparent reduction in the piston velocity is the effect of resonance fluorescence on the shape and peak intensity of the piston. The differences in these properties between Figs. 4(a) and 4(b) are significant. Whereas the piston achieves a maximum intensity of $\sim 3\times 10^{13}$ cm^{-3} in Fig. 4(a), the corresponding value is only $\sim 6\times 10^{12}$ cm^{-3} in Fig. 4(b). It is noted that the value predicted by WHW Eq. (20) for this case is also $\sim 3\times 10^{13}$ cm^{-3}. Moreover, the experimentally observed shape of the piston (e.g., presented in WHW Fig. 4) is much closer to that observed in the (b) and (c) panels of Figs. 4 and 5 than that shown in the nonfluorescence (a) panels.

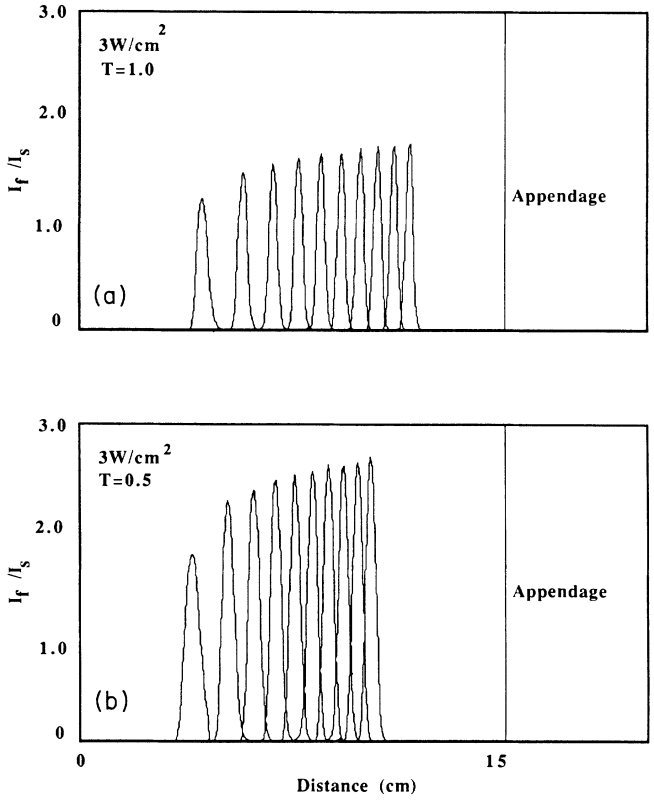

FIG. 6. Fluorescence distributions for optical-piston propagation calculated using the current model [i.e., Eq. (3) for v_d, Eq. (13) with saturation, Eq. (16), and boundary conditions (14a) and (14b)] *with* resonance-fluorescence effects for $I_0=3.0$ W/cm^2; $\alpha=40,\gamma=454$; and equal time increments of $\theta=10^{-2}$. (a) $T=1.0$; (b) $T=0.5$.

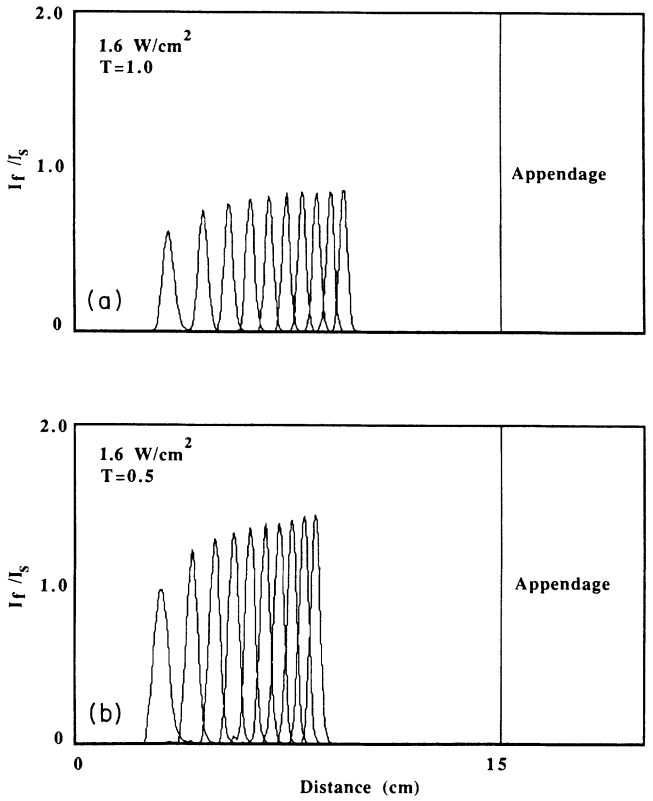

FIG. 7. Fluorescence distributions for optical-piston propagation calculated using the current model [i.e., Eq. (3) for v_d, Eq. (13) with saturation, Eq. (16), and boundary conditions (14a) and (14b)] *with* resonance-fluorescence effects for $I_0=1.6$ W/cm^2; $\alpha=40,\gamma=320$; and equal time increments of $\theta=10^{-2}$. (a) Base case, Fig. 2(b) results; (b) $T=1.0$; (c) $T=0.5$.

IV. CONCLUSIONS

From the results presented above, it is concluded that for the typical experimental conditions of WHW, the Na density wave of the optical piston never attains a "self-preserving" form during its traverse of the diffusion cell, i.e., both the velocity and the shape of the traveling density distribution change continuously with time. It is shown, however, that the conditions of a finite number of absorbers in an infinite medium can indeed produce a density wave that preserves its form, and that this holds true for both saturated and unsaturated conditions.

Also, using the formulation developed here, it has been shown that resonance fluorescence acts to significantly reduce the optical-piston velocity, broaden the density distribution, and decrease its peak height. Therefore, it is concluded that resonance fluorescence can play a significant role in determining the time evolution and detailed shape of the optical-piston density distribution in sodium, and that it must be considered in any model that attempts to explain the detailed dynamics of the optical piston.

ACKNOWLEDGMENTS

One of us (N.M.L.) gratefully acknowledges partial financial support from the Alfred P. Sloan Foundation and the National Science Foundation.

---

*To whom all correspondence should be addressed.

[1]H. G. C. Werij, J. P. Woerdman, J. J. M. Beenakker, and I. Kuscer, Phys. Rev. Lett. **52**, 2237 (1984).

[2]H. G. C. Werij, J. E. M. Haverkort, and J. P. Woerdman, Phys. Rev. A **33**, 3270 (1986).

[3]J. E. M. Haverkort, *Light-Induced Drift of Na in Noble Gases: A Realistic Description,* Doctoral Dissertation, University of Leiden, The Netherlands, 1987.

[4]F. Kh. Gel'mukhanov and A. M. Shalagin, Pis'ma Zh. Eksp. Teor. Fiz. **29**, 711 (1979) [Sov. Phys.—JETP Lett. **29**, 711 (1979)].

[5]F. Kh. Gel'mukhanov and A. M. Shalagin, Zh. Eksp. Teor. Fiz. **78**, 1674 (1980) [Sov. Phys.—JETP **51**, 839 (1980)].

[6]H. G. C. Werij, J. E. M. Haverkort, P. C. M. Planken, E. R. Eliel, J. P. Woerdman, S. N. Atutov, P. L. Chapovskii, and F. Kh. Gel'mukhanov (unpublished).

[7]J. H. Xu, M. Allegrini, S. Gozzini, E. Mariotti, and L. Moi, Opt. Commun. **63**, 43 (1987).

[8]W. A. Hamel, A. D. Streater, and J. P. Woerdman, Opt. Commun. **63**, 32 (1987).

[9]N. M. Lawandy, IEEE J. Quantum Electron. **QE-22**, 1003 (1986).

[10]N. K. Madsen and R. F. Sincovec, ACM Trans. Math. Software **5**, 326 (1979).

[11]G. Nienhuis, Phys. Rev. A **31**, 1636 (1985).

[12]G. Nienhuis, Phys. Rep. **138**, 151 (1986).